

Article

Dynamic Wireless Power Transfer for Warehouse Robots

Jiropast Suakaew^a and Wanchai Pijitrojana^{b,*}

Department of Electrical and Computer Engineering, Thammasat School of Engineering,
Thammasat University, Klongluang, Pathumthani 12121, Thailand

E-mail: ^ajiropast.suakaew@gmail.com, ^{b,*}pwanchai@engr.tu.ac.th (Corresponding author)

Abstract. The possible wireless power transfer (WPT) consists of stationary and dynamic wireless power transfer (DWPT) for warehouse robots power charging. The stationary wireless charging for warehouse robots has several disadvantages of long charging time, non-running, frequent charging, etc., whereas DWPT is a broad application prospect and is considered one of the best solutions above-stated problems. This paper proposes a maximum transfer efficiency and distance method in the DWPT for Warehouse Robots using a magnetic resonant (MR) inductive coupling subsection coil powered by a transmitter coil (Tx). The optimal efficiency is reached when three adjacent subsection coil (SC) are simultaneously powered on a single Tx. The two critical parameters in DWPT are Power Delivered to the Load (PDL) and Power Transfer Efficiency (PTE). The design results of an MR inductive coupling and a magnetic resonant inductive coupling subsection coil (MRSC) WPT optimized for a 20 kHz operating frequency at 8-cm, 11-cm, and 16-cm coupling distance show PTE (an MR inductive/MRSC) WPT of 85/87%, 65/70%, 45/65%, respectively, and the PDL of the MRSC WPT 3.2%, 11.1%, and 50% respectively higher than an MR inductive WPT. Results also show that the robot moves smoothly along the transmission track, and having the MRSC underneath is a less complicated system.

Keywords: Magnetic resonance, dynamic wireless charging system, wireless power transfer, warehouse robots.

ENGINEERING JOURNAL Volume 25 Issue 10

Received 27 January 2021

Accepted 12 October 2021

Published 31 October 2021

Online at <https://engj.org/>

DOI:10.4186/ej.2021.25.10.61

1. Introduction

The logistic technology for products is becoming a widely used technology; more warehouses are utilizing robotics technology. The U.S. market [1] of warehouse robotics by 2022 will grow \$6 billion, 11.8% CAGR (Compound Annual Growth Rate) between 2017 and 2022. Robots that do not need to be charged can work longer than the human competition, so wireless power is game-changing in the robotics field. The development of electronic components, the technology that charges the robots while driving for an operation, has a promising function, flexible, and reduces onboard battery requirement. The onboard battery capacity limited an extended time of deployment of mobile robots. Technological advances have increased the efficiency of batteries and their energy capacity. The batteries have been manually replaced at a base station for mobile robots is an option of their limitation. Wireless power transfer (WPT) technologies can be considered because they are flexible, safe, free of dust/dirt, and enable in the motion charging system. The advantages include power delivered to the load (PDL) and power transfer efficiency (PTE), eliminating sparks from contacts, and no need to use a tether.

Wireless power transfer (WPT) technology is one of the most prosperous research areas for many researchers and engineers since the emergence of Witricity. The Wireless charging system is classified into static wireless charging (SWC) and Dynamic wireless charging (DWC). SWC consists of the receiver side, which needs to be aligned correctly in the static position with the transmitter, which then delivers power to the battery, while in DWC, the battery is going to be charged while the vehicle is in motion. The battery capacity issues and energy density issues limit the development of the SWC [2]. Thus, the DWC enables the transmission of electrical power through the air to an electric vehicle in motion and is considered one of the best solutions for minimizing battery life and increasing the range of travel [3-4]. The DWC can be implemented either through a subsection coil (SC) or a long track mounted over the road length. Figure 1 shows subsection pads DWC in which multiple subsection pads that are used as a transmitter are buried under the surface of the road while a secondary pad or receiver is mounted on the vehicle. As robots travel over the pads, the transmission track charges the battery, increasing the robots' range, and the coupling coefficient is energized, thus reducing losses, EMI emission, and improving system efficiency.

Detection of a robot in subsection pads DWC is one of the foremost issues as it travels on the road and turns on the appropriate pad [5]. DWC set-up can differ between the high-speed and low-speed set-up.

The high-speed set-up, such as freeways, automobiles pass over the Tx, which activates in fractions of a second, but the time for the Tx to power the Rx is limited, which

is also a considerable challenge for the DWC system due to the fast variation of load [6].

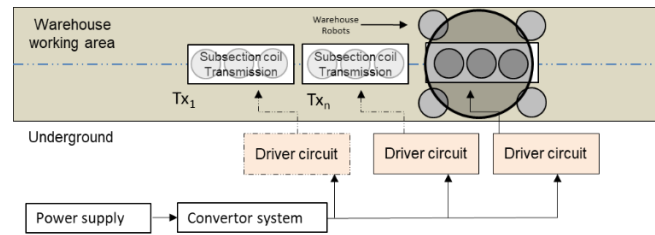


Fig. 1. Power supply connection to underground transmitting pads.

In the low-speed set-up, the automobiles will slow down when reaching the bus stop or traffic light and then speed up at the time of leaving. They can be charged when they enter the charging section area without even stopping due to the transmitters installed. The quality factor "Q" and coupling coefficient "K" between the transmitter and receiver are two important parameters upon which the efficiency " η " of a system depends. Higher "Q" means low energy loss rate, while higher coupling rate "K" can lead to higher efficiency " η " of a system [7]. MR inductive coil designs simplify system control and provide a relatively constant coupling coefficient as the vehicle moves in the designated area, but they suffer from the field emitted in the coil's uncoupled area due to the sizeable uncoupled flux of the transmitter coil, which results in low efficiency. In [8], the authors present a method for SWC by designing a new Tx coil, which is more effective than an MR inductive coil system. In [9], multiple transmitter pads are used to signify the working of DWC to transfer power to the load; however, the experimental arrangement is not magnetically optimized and complicates the Tx system.

This paper proposes a system of increased transfer efficiency in DWC with three adjacent SCs are simultaneously powered on a single Tx magnetically optimized for more space utilization. The system transfers power using generated magnetic fields from MRSC on the Tx to the receiver (Rx) coil. The idea behind efficiency improvement is the coupling of the magnetic from Tx to MRSC coil with a lesser current in the Tx coil to encourage a significant current in the MRSC coil to produce magnetic flux to Rx, thus increasing the system efficiency and reducing the leakage EMF which can be achieved in the system. The MRSC on the Tx overcomes the MR inductive coil WPT's limitations with more space utilization [10-13].

The paper is organized as follows. The transmitter system's design and the equations that describe the equivalent circuit are derived and validated by simulation in section 2. The experimental setup is shown in section 3, whereas the results' discussion and conclusions are given in the last section.

2. Theory of MRSC Coupled Coils

2.1. Transmitting with MRSC Coupled Coil Concept

This system is considered a periodical array of Tx. Tx coil can switch on and off depending on the position of the Rx. The paper aims to present the optimal transmitting system, and a single Tx has activated three adjacent MRSC coils, which is to overcome the previous study of only a single coil. In [14], optimal efficiency is reached when three adjacent same sizes Tx MRSC coils simultaneously contribute flux linkage to Rx. An advantage of this adjacent MRSC coil is the improved system efficiency since losses in the Tx are reduced. From [15], when the sizes of the single Tx and Rx antenna coils are the same, the simulation shows that we obtain higher magnetic field strength.

In this paper, the transmitting MRSC, designed and fabricated entirely into the system, MRSC coil receives the magnetic field from the Tx coil which has been implemented on the transmitter side and enhance magnetic field to the Rx coil, it comprises an array of metallic spiral coils with capacitor loading to the circuit. Figure 2 shows the front view of the Tx coil with the embedded three adjacent MRSC coils. An external RF field induced the synergy to the magnetic MRSC, the induced current in the resonant mode leads to significant improvements in the magnetic field.

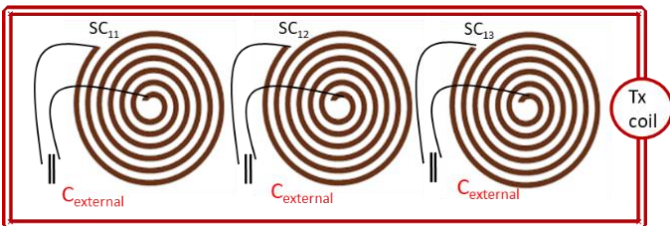
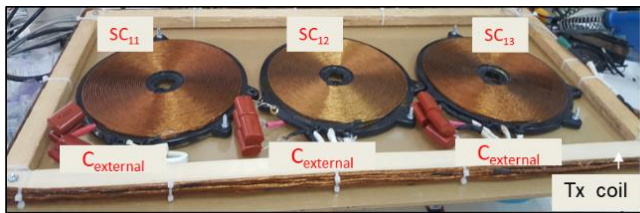


Fig. 2. Schematic MRSC structure is composed of an array featuring metallic spiral coils with a capacitor loading to the circuit.

The characteristic of Tx with MRSC defines the efficiency and overall performance of the system. The MRSC implemented on the Tx coil delivers the accumulative assistances of the coupling coefficient of the system. Applying [16] the simple 2-coil MR inductive is encompassed to an m -coil Tx, in which 1^{st} and m^{th} coils are organized to the energy source and load. The reflected load from the $(j + 1)^{th}$ coil to the j^{th} coil is given by Eq. (1).

$$R_{ref\ j,j+1} = k_{j,j+1}^2 \omega_0 L_j Q_{(j+1)L}, j = 1, 2, 3, \dots, m - 1 \quad (1)$$

where $k_{j,j+1}$ is the coupling coefficient between the j^{th} and $(j + 1)^{th}$ coils and all coils are adjusted at the equivalent working frequency $f_0 \cdot Q_{(j+1)L}$ because the loaded quality factor of the $(j + 1)^{th}$ coil can be defined using Eq. (2).

$$Q_{jL} = \frac{\omega_0 L_j}{R_j + R_{ref\ j,j+1}} = \frac{Q_j}{1 + k_{j,j+1}^2 Q_j Q_{(j+1)L}}, j = 1, 2, \dots, m - 1 \quad (2)$$

The unloaded quality factor is $Q_j = \omega_0 L_j / R_j$ and the parasitic series resistance of the j^{th} coil is R_j . It is negligible the coupling between non-neighboring coils, the power transfer efficiency from the j^{th} coil to the $(j + 1)^{th}$ coil can be defined using Eq. (3).

$$\eta_{j,j+1} = \frac{R_{ref\ j,j+1}}{R_j + R_{ref\ j,j+1}} = \frac{k_{j,j+1}^2 Q_j Q_{(j+1)L}}{1 + k_{j,j+1}^2 Q_j Q_{(j+1)L}} \quad (3)$$

Overall power transfer efficiency (PTE) in several-coil can be defined using Eq. (4).

$$\eta_{m-coil} = \prod_{j=1}^{m-1} \eta_{j,j+1} \frac{Q_{mL}}{Q_L} \quad (4)$$

Furthermore, the power delivered to the load (PDL) is given by Eq. (5).

$$P_{L,m-coil} = \frac{V_s^2}{2R_{Tx}} \frac{1}{1 + k_{12}^2 Q_{Tx} Q_{RxL}} \eta_{m-coil} \quad (5)$$

2.2. System Efficiency

The transfer distance, coupling coefficient, and operating frequency have improved by the MRSC coil structure. The MRSC coil optimum position is located nearby the Tx coil [9]. The mutual and self-inductance have been enhancements at the Tx with the MRSC coil at the resonance frequency. Figure 3 (a) shows the circuit diagram of the Tx, Rx and, MRSC WPT system where self-inductance is L_1 and L_2 . Figure 3 (b) is the transformer model circuit diagram that explains the transfer function of the input and output. It is advantageous to examine the power transfer efficiency, out/input impedances. The transfer efficiency has been increased by the coupling coefficient and the effective inductance Z_{L1} . The WPT resonance frequency ω_t of WPT with the MRSC coil can be defined using Eq. (6).

$$\omega_t = \frac{1}{\sqrt{C_{sc}(L_{sc} + \frac{L_m}{m^2})}} \quad (6)$$

The operating frequency can be approximated theoretically based on the formula given in Eq. (6),

which gives an operating frequency of $f = 20$ kHz.

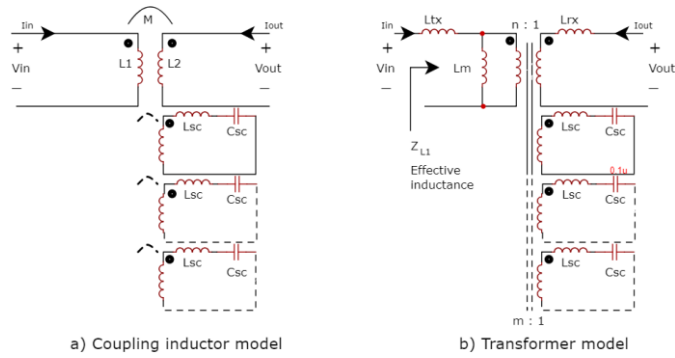


Fig. 3. Circuit diagram of the Tx and Rx WPT system with the MRSC coil.

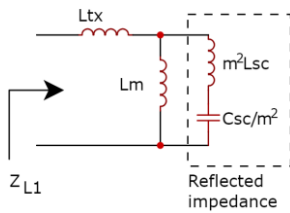


Fig. 4. The equivalent circuit of the effective inductance.

The equivalent circuit Z_{L1} is illustrated in Fig. 4, where the MRSC coil reflected impedance denominates the Tx, Z_{L1} which can be defined using equation (7) and Table 1.

$$Z_{L1} = \left| \frac{s^3 (L_{tx}(m^2 L_{sc} + L_m) + m^2 L_m L_{sc}) \frac{C_{sc}}{m^2} + s(L_m + L_{tx})}{s^2 (L_{sc} + \frac{L_m}{m^2}) C_{sc} + 1} \right| \quad (7)$$

Table 1. Terms of the resonance frequency.

S.no	Terms	Abbreviations
1	ω_t	Resonance frequency
2	C_{sc}	The capacitance of the MRSC coil
3	L_{sc}	The inductance of the MRSC coil
4	L_m	Mutual inductance of a coil

The MRSC WPT circuit diagram of the Tx and Rx is shown in Fig. 5. The AC equivalent circuit has illustrated in Fig. 6, and the MRSC coil reflected impedance has been embedded in the structure. Consequently, M_2 is the voltage transfer function of the MRSC structure. The system's voltage transfer function that has been added by the MRSC structure can be defined using Eq. (8).

$$M_2 = M \left| \frac{Z_c}{Z_c + Z_A || L_m || (Z_b + R_{ac})} \right| \quad (8)$$

Depending on the MRSC coil effect's influence, the voltage gain increases when compared with the MR inductive WPT system. The voltage transfer function of the MR inductive WPT system, M for which $M = nV_{out}/V_{in}$.

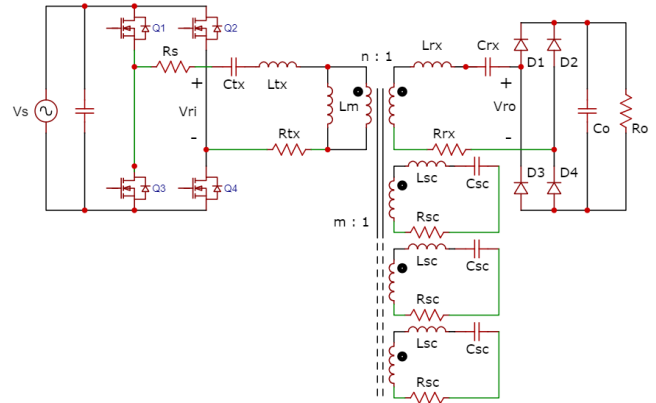


Fig. 5. The Tx and Rx WPT system with the MRSC coil.

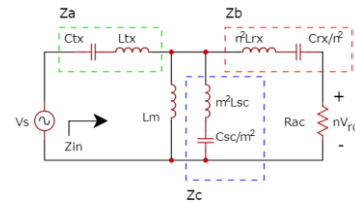


Fig. 6. The AC equivalent circuit with the MRSC coil.

2.3. The Transmission Design with Optimizing Consideration

The Tx coil can be energized by an excitation source [17-20]. An effective inductance and capacitance L and C for each coil can be defined using Eq. (9)-(11).

$$L_{ij} = \frac{\mu_0}{4\pi |I_i I_j|} \iint dr_i dr_j \frac{j(r_i) \cdot j(r_j)}{|r_i - r_j|} \quad (9)$$

$$\frac{1}{C} = \frac{1}{4\pi \epsilon_0 |q_o|^2} \iint dr_i dr_j \frac{\rho(r_i) \cdot \rho(r_j)}{|r_i - r_j|} \quad (10)$$

$$C_{total} = C_{intrinsic} + C_{external} \quad (11)$$

Equations (9)-(11) represent the effective self-inductance and capacitance of a discrete unit cell where the spatial current $j(r)$ and charge density $\rho(r)$ are obtained respectively from the current and charge densities along with the isolated coil, in conjunction with the geometry of the object [7]. The MRSC consists of Litz spiral winding having an outer diameter and a cell distance of 8 cm. and 2 cm, respectively. A compensator capacitance determines the working frequency and low sensitivity to the external objects, the effective inductance and capacitance of 140μH and 0.47μF, respectively.

The MRSC's magnetic field enhancement and operating frequency has been derived by employing the coupled-mode theory [21]. The periodic boundary condition simulation analysis was conducted to derive the behavior of operating frequency and transmission efficiency between adjacent unit cells. Figure 7 shows the periodic boundary condition simulation of an MRSC ordered as 1×3 arrays, in [22] to cover the Rx range. The operating frequency and magnetic field enhancement results between the adjacent unit cells are shown in Fig. 8. The operating frequency and magnetic field enhancement are gradually shifted when the ratio d/D is up to 15%. The mutual MR inductive coupling from the neighboring MRSC affects total inductance, and operating frequency goes down.

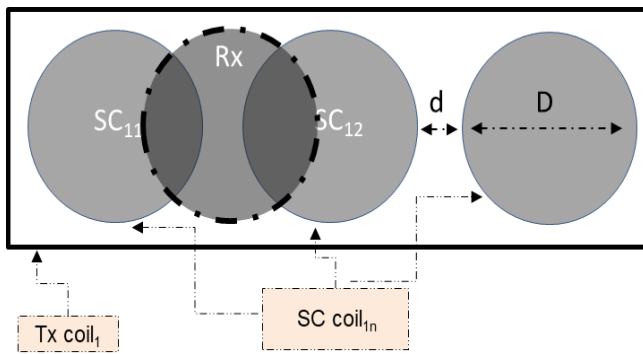


Fig. 7. Periodic boundary condition simulation of the MRSC transmission design, 1×3 arrays with an air gap Tx and Rx coil at 16 cm.

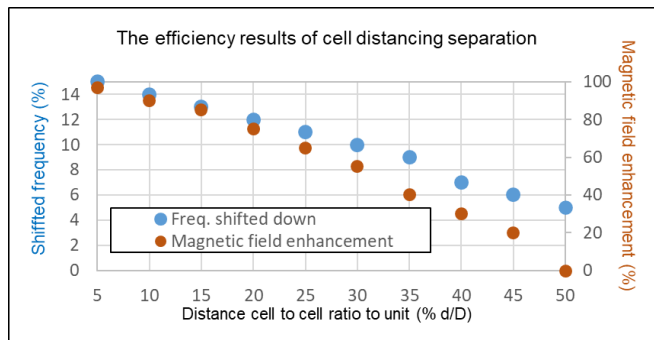


Fig. 8. Efficiency results of separation of cell distance from adjacent MRSC unit cells.

3. Circuit Analysis and Experimental Set-Up

3.1. The Lumped Element Circuit Analysis

To examine an MR inductive WPT and MRSC WPT structures from the PTE and PDL for an extended distance. The model has been proved by circuit analysis and experimental set-up obtained from practical prototypes.

3.1.1. A MR inductive WPT

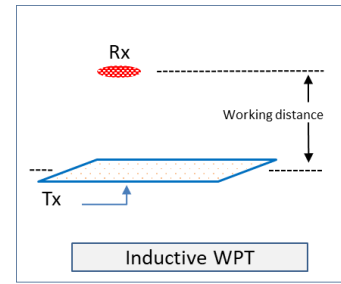


Fig. 9. An MR inductive WPT structure is consists of two LC resonators.

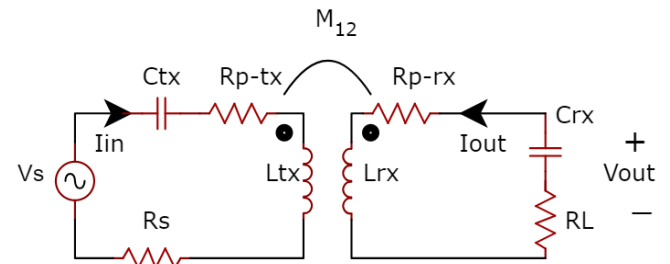


Fig. 10. Circuit diagram of the Tx and Rx WPT system.

Figure 9 shows the arrangement of an MR inductive WPT structure. Each coil has formed a resonance frequency with a series capacitor. The transmitter and receiver coils have used a capacitor to counterbalance the stray inductance. The increased working distance is reduced the system energy efficiency of such an MR inductive WPT system [8]. The lumped element circuit of an MR inductive WPT structure of Fig. 9 is illustrated in Fig. 10. Equations (12)-(13) represent the circuit equation.

$$((R_s + R_{p-tx}) + jX_{in})I_{in} + j\omega M_{12}I_{out} = V_s \quad (12)$$

$$j\omega M_{12}I_{in} + ((R_L + R_{p-rx}) + jX_{out})I_{out} = 0 \quad (13)$$

where R_s is the source resistance and the parasitic resistance of the Tx is R_{p-tx} ; The load resistance is R_L and the parasitic resistance of the Rx is R_{p-rx} ; The reactance is $X_{in} = \omega L_{tx} - 1/(\omega C_{tx})$; The inductance is L_{tx} , the Tx capacitance is C_{tx} , and the current in the resonator is I_{in} ; the voltage source is V_s ; The resonators mutual inductance between Tx and Rx is M_{12} ; The angular frequency is ω . The model at the resonance frequency, $X_{in} = X_{out} = 0$. The system has operated in resonance frequency to maximize the power transfer capability of this structure. The energy efficiency of a MR inductive system can be defined by Eq. (14).

$$\eta = \eta_{Tx}\eta_{Rx} \quad (14)$$

$$\eta_{Tx} = \frac{R_{Tx}}{R_s + R_{p-tx} + R_{Tx}}, R_{Tx} = \frac{\omega^2 M_{12}^2}{(R_L + R_{p-rx})} \quad (15)$$

Equation (15) expresses the transmitter's energy efficiency η_{Tx} , where the reflected resistance Rx to Tx is R_{Tx} .

$$\eta_{Rx} = \frac{R_L}{R_L + R_{P-rx}} \quad (16)$$

Equation (16) is the efficiency of the receiver, η_{Rx} . However, to maximize η_{Tx} , R_S and R_{P-rx} is small and R_{Tx} is extensive. A large R_{Tx} implies that M_{12} is big at the operating frequency. If the distance between the Tx and the Rx increases, then PTE reduces the system energy efficiency of such an MR inductive WPT system.

3.1.2. The MRSC transmitting WPT

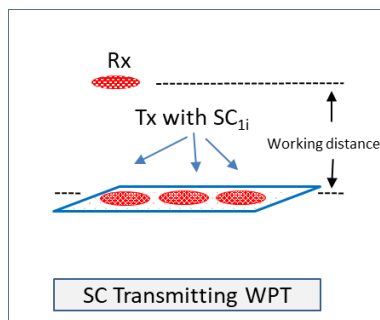


Fig. 11. The MRSC WPT system consists of SC coils.

In this section, it is proposed that the structure of the MRSC transmitting determines the key factors that target maximum power transfer frequency. Figure 11 shows the MRSC WPT system containing SC coils at the transmitter side. The MRSC WPT system replaces weak energy effectiveness for an MR inductive WPT with lengthy transfer space.

The MRSC WPT system is supported that the offered structure's efficiency, under precise structure circumstances, has been better than that of an MR inductive WPT system. The SC coil auxiliary to the Tx side of the initial an MR inductive structure becomes a repeater or a relay. A Lize coil connected in series with a resonant capacitor to form a coil resonator is the MRSC coil structure. For easiness, The effect of magnetic coupling between the Tx coil to the receiver Rx of the extended transfer distance is insignificantly compared to the SC coil's magnetic coupling effect to Rx. The Tx, Rx, and SC are operated at the resonant frequency $X_{Tx} = X_{SC} = X_{Rx} = 0$, the calculation term of the system are given by Eq. (17)-(19).

$$(R_S + R_{Tx})I_{in} + j\omega M_{TxSC}I_{SC} = V_S \quad (17)$$

$$j\omega M_{TxSC}I_{in} + R_{SC}I_{SC} + j\omega M_{RxSC}I_{out} = 0 \quad (18)$$

$$j\omega M_{RxSC}I_{SC} + (R_L + R_{Rx})I_{out} = 0 \quad (19)$$

The terms used in the lumped circuit elements are shown in Table 2.

Table 2. Terms of the lumped circuit.

S.no	Terms	Abbreviations
1	R_S, R_L	Source / Load resistance
2	R_{Tx}	Transmission coil resistance
3	R_{SC}	SC coil resistance
4	R_{Rx}	Receiving coil resistance
5	M_{TxSC}	Mutual inductance between the Tx coil and SC coils
6	M_{RxSC}	Mutual Inductance between Rx coil and SC coils
7	I_{in}	Transmission coil current
8	I_{out}	Receiving coil current
9	I_{SC}	SC coil current
10	η'	The total efficiency of the MRSC WPT
11	η	The total efficiency of a MR inductive WPT
12	η_{Tx}	Transmission coil efficiency
13	η_{SC}	Metamaterial coil efficiency
14	η_{Rx}	Receiving coil efficiency

Equations (20-23) represent the energy efficiencies of the MRSC WPT system. Also, Tx and Rx reflected resistances are given by Eq. (24)-(25).

$$\eta' = \eta_{Tx}\eta_{SC}\eta_{Rx} \quad (20)$$

$$\eta_{Tx} = \frac{R_{TxSC}}{R_S + R_{P-Tx} + R_{TxSC}} \quad (21)$$

$$\eta_{SC} = \frac{R_{TxSC}}{R_{SC} + R_{TxSC}} \quad (22)$$

$$\eta_{Rx} = \frac{R_L}{R_L + R_{P-rx}} \quad (23)$$

The terms used in the reflected resistances are shown in Table 3.

Table 3. Terms of the reflected resistance.

S.no	Terms	Abbreviations
1	R_{TxSC}	Reflected resistance from SC coil to Tx coil
2	R_{RxSC}	Reflected resistance from receiving coil to SC coil

$$R_{TxSC} = \frac{\omega^2 M_{TxSC}^2}{R_{Ptx} + R_{RxSC}} \quad (24)$$

$$R_{RxSC} = \frac{\omega^2 M_{RxSC}^2}{R_L} \quad (25)$$

The following inequality can be expressed by equation (26) for the MRSC WPT system's energy effectiveness to be improved over a MR inductive WPT system.

$$\eta' > \eta \quad (26)$$

Equations (17)-(25) provide the calculation term of the system, Eq. (26) specifies the MRSC WPT system's energy

effectiveness to be improved over a MR inductive WPT system.

3.2. Experimental Set-up

An experimental set-up of the system is shown in Figs. 12 and 13 consist of the high frequency (HF) H-bridge inverter, a power supply, AC to DC converter on the Tx, while the receiver side consists of an Rx coil mounted underneath the robot with DC to DC controller, AC to DC filtering, a diode bridge rectifier, a resonant tuning capacitor connected directly to the load.

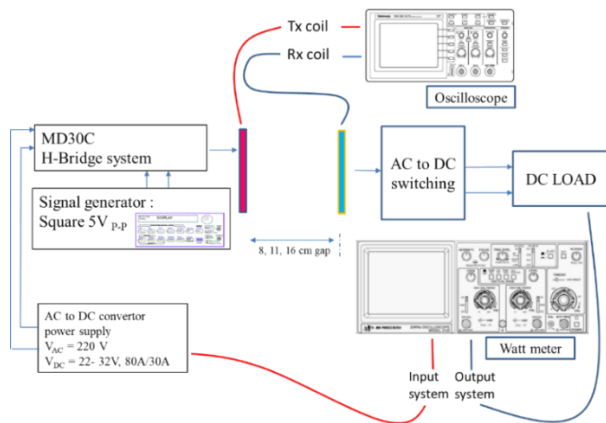
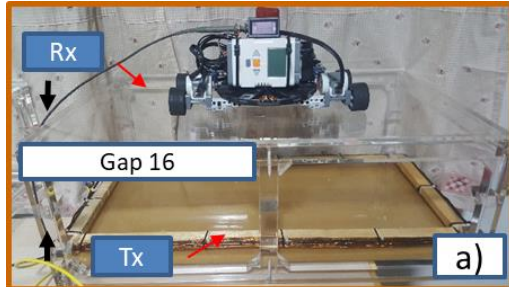
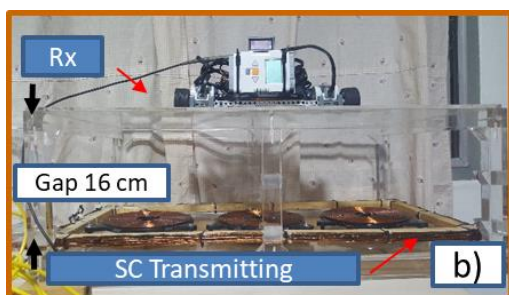


Fig. 12. Experimental set-up for the WPT System.



a) An MR inductive WPT.



b) MRSC Transmitting WPT.

Fig. 13. An experimental set-up for different operating air gaps in the system. a) A MR inductive WPT b) MRSC Transmitting WPT.

The Tx and Rx coil's transmission efficiencies compared between an MR inductive and the MRSC transmitting WPT system. The working frequency was

preferred to be the frequency at which it became boosted between the Tx and Rx. The MRSC transmitting structure showed performance compared to an MR inductive system at an air gap of 8, 11, and 16 cm away from the Tx coil. The PDL of the MRSC WPT was 3.2%, 11.1%, and 50% higher than an MR inductive WPT. An MR inductive WPT and the MRSC transmitting WPT at 8-cm, 11-cm, and 16-cm coupling distance showed PTE (An MR inductive/MRSC WPT) of 85/87%, 65/70%, 45/65%, respectively, as shown in Table 4.

Table 4. Measurement results of PDL and PTE efficiency.

System set up		System efficiency (%)		
Type	Gap (cm.)	MR WPT	MRSC WPT	MRSC to MR improvement
PTE	8	85	87	2
	11	65	70	7
	16	45	65	31
PDL	8	60	62	3
	11	40	45	11
	16	20	40	50

The measurements are obtained at nine different positions, as shown in Fig. 14. The receiver coil underneath the robot moves through the different positions. These positions are P1) Right before alignment

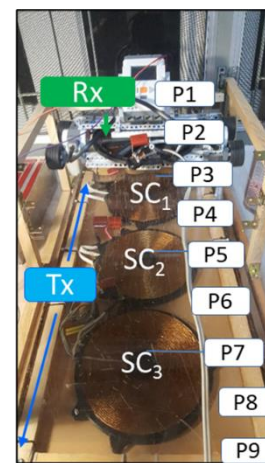


Fig. 14. shows the movements of the Rx coil underneath of the robot through the different positions.

with the first SC coil, edge to edge. P2) 50% aligned with the first SC coil. P3) Perfectly aligned with the first SC coil. P4) 50% misaligned with the first SC coil towards the second SC coil. P5) Perfectly aligned with the second SC coil, position. P6) 50% aligned with the second SC coil. P7) Perfectly aligned with the third SC coil. P8) 50% misaligned with the third SC coil. P9) Right after alignment with the third SC coil, edge to edge.

The power transfer efficiencies of the Rx coil at different positions are shown in Fig. 15. The MRSC-based transmitter WPT system operates at the optimized

frequency of 20 kHz, so that the efficiency of the MRSC based WPT is higher than an inductive based WPT.

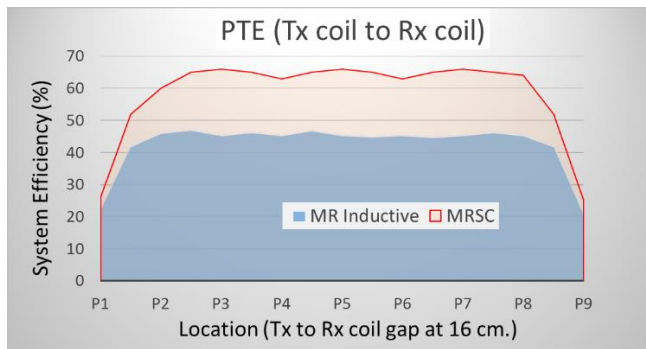


Fig. 15. Experimental results of the system and the measurements obtained at the different positions.

To demonstrate the ability of DWPT using the MRSC for transmitting. A railroad of 1.2m long was used in this experiment. The MRSC transmitting was fabricated with the railroad, consisting of a Litz spiral winding. The Tx and Rx is a vertical distance of 16 cm. A study was implemented with a 20 W robot moving on the railroad to validate the dynamic WPT flexibility at an operating frequency of 20 kHz. The capacitance and inductance of the MRSC cell were set at $0.47 \mu\text{F}$ and $140 \mu\text{H}$, respectively. When the MRSC transmitting was implemented, the Tx structure was located underneath the railroad for testing with the HF inverter powered to the array via the Tx coil embedded with the three adjacent MRSC. The robot's battery was disconnected and substituted by electronic circuits for power delivered to the Rx robot. The system's apparatuses shown in Fig. 16 included a modified MD30C used as an HF power supply and capable of a frequency up to 30 MHz.

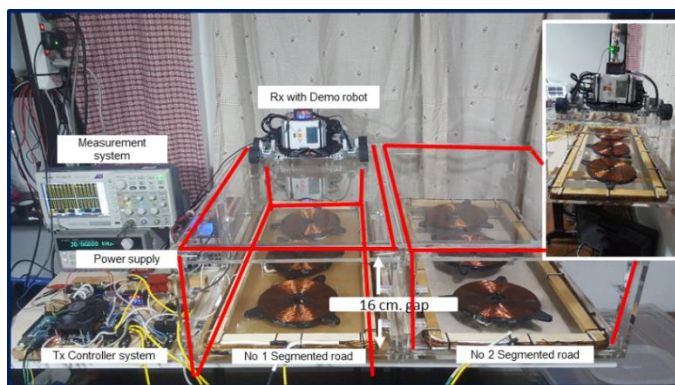


Fig. 16 DWPT MRSC experimental set up with an array of the rail MRSC transmitting WPT system, having 1.2m long track.

The robot could endlessly length the road with the DWPT using the MRSC system, and no need to push the robot physically on the road. To activate a single MRSC at a time of power optimization when the robot arrives. A data network can be an arrangement between the Tx and Rx for the system closed-loop stabilizer. In [23], the authors

present a robust and efficient DWPT by using a switch-mode implementation. However, this approach requires an amplifier circuit with current-sensing feedback. It can also be flexible and a useful wireless power delivery solution for future work.

4. Conclusion

The proposed research work presents a novel approach for improving the DWPT system by using three adjacent MRSC are simultaneously powered on a single Tx. The MRSC transmitting is derived from the sub-units embedded on the transmitter side to improve the efficiency of the system. Equations (4) and (5) represent the PTE and PDL. Design examples of an MR inductive WPT and MRSC transmitting WPT have been presented and optimized for a 20 kHz operating frequency at 8-cm, 11-cm, and 16-cm coupling distance, showing PTE (an MR inductive/MRSC) WPT of 85/87%, 65/70%, 45/65%, respectively. The MRSC comprises an array of a metallic spiral coils with a capacitor loading to reduce the system's size. The MRSC transmitting can be properly implemented on the transmitting side in a horizontal layout of the DWPT system. At the distance of 8-cm, 11-cm, and 16-cm, PDL of the MRSC WPT is 3.2%, 11.1%, and 50% higher than an MR inductive WPT and improves wireless power transfer in terms of efficiency, range, and flexibility, and also increases the coupling coefficient between the Tx and Rx coils. Moreover, the system can transfer power dynamically to battery charging vehicles on the roads, mobile devices, and warehouse robots.

References

- [1] W. Allen, *The Business Case for Collaborative Mobile Robotics*. 6 River Systems, October 19, 2020
- [2] N. T. Diep, N. K. Trung, and T. T. Minh, "Maximum efficiency in the dynamic wireless charging systems of electric vehicles," in *2019 10th International Conference on Power Electronics and ECCE Asia (ICPE 2019 - ECCE Asia)*, Busan, Korea (South), 2019, pp. 1-6.
- [3] C. C. Mi, G. Buja, S. Y. Choi, and C. T. Rim, "Modern advances in wireless power transfer systems for roadway powered electric vehicles," *IEEE Trans. Ind. Electron.*, vol. 63, no. 10, pp. 6533-6545, Oct. 2016.
- [4] W. C. Cheah, S. A. Watson, and Ba. Lennox, *Limitations of Wireless Power Transfer Technologies for Mobile Robots*. Cambridge University Press, 2019.
- [5] A. Gil, P. Sauras-Perez, and J. Taiber, "Communication requirements for dynamic wireless power transfer for battery electric vehicles," in *Electric Vehicle Conference (IEVC)*, 2014 IEEE International, 2014, pp. 1-7.
- [6] A. A. S. Mohamed, C. R. Lashway, and O. Mohammed, "Modeling and feasibility analysis of quasi-dynamic WPT system for EV applications,"

- IEEE Trans. Transport. Electrification*, vol. 3, no. 2, pp. 343–353, Jun. 2017.
- [7] A. Kurs, A. Karalis, R. Moffatt, J. D. Joannopoulos, P. Fisher, and M. Soljic, “Wireless power transfer via strongly coupled magnetic resonances,” *Science*, vol. 317, pp. 83–86, 2007.
- [8] W. X. Zhong, C. Zhang, X. Liu, and S.R. Hui, “A methodology for making a three-coil wireless power transfer system more energy efficient than a two-coil counterpart for extended transfer distance,” *IEEE Trans. Power Electron.*, vol. 30, no. 2, Feb. 2015.
- [9] K. Lee, Z. Pantic, and S. M. Lukic, “Reflexive field containment in dynamic inductive power transfer systems,” *IEEE Transactions on Power Electronics*, vol. 29, pp. 4592-4602 no. 9, Sep. 2014
- [10] Y. Cho, S. Lee, D.-H. Kim, H. Kim, C. Song, S. Kong, J. Park, C. Seo, and J. Kim, “Thin hybrid metamaterial slab with negative and zero permeability for high efficiency and low electromagnetic field in wireless power transfer systems,” *IEEE Transactions on Industrial Electronics*, vol. 60, no. 4, pp. 1001-1009, Aug. 2018.
- [11] B. Wang, T. Nishino, and K. H. Teo, “Wireless power transmission efficiency enhancement with metamaterials,” in *Proc. IEEE Int. Conf. Wireless Inf. Technol. Syst.*, Honolulu, HI, USA, Aug. 28–Sep. 3, 2010, doi:10.1109/ICWITS.2010.5612284.
- [12] Y. Urzhumov and D. R. Smith, “Metamaterial-enhanced coupling between magnetic dipoles for efficient wireless power transfer,” *Phys. Rev. B*, vol. 83, no. 20, p. 205114, 2011.
- [13] B. Wang, K. H. Teo, T. Nishino, W. Yezunis, J. Barnwell, and J. Zhang, “Wireless power transfer with metamaterials,” in *Proc. Eur. Conf. Antennas Propag.*, Rome, Italy, Apr. 11–15, 2011, pp. 3905–3908.
- [14] J. P. C. Smeets, T. T. Overboom, J. W. Jansen, and E. A. Lomonova, “Modeling framework for contactless energy transfer systems for linear actuators,” *IEEE Trans. Ind. Electron.*, vol. 60, no. 1, Jan. 2013.
- [15] J. Suakaew and W. Pijitrojana, “A dynamic wireless power transfer using metamaterial-based transmitter,” *Progress In Electromagnetics Research C*, vol. 110, 151–165, 2021.
- [16] M. Kiani, U. M. Jow, and Maysam Ghovanloo, “Design and optimization of a 3-coil inductive link for efficient wireless power transmission,” *IEEE Transactions on Biomedical Circuits and Systems*, vol. 5, no 6, pp.579-591, Dec. 2011.
- [17] A. Rittiplang and W. Pijitrojana, “A low-frequency wireless power transfer using parallel resonance under impedance matching,” *Applied Mechanics and Material*, vol. 781, pp. 410-413, Aug. 2015.
- [18] A. Rittiplang and W. Pijitrojana, “Low-frequency wireless power transfer using optimal primary capacitance of parallel resonance for impedance matching,” *IJIREEICE*, vol. 4, no. 1, Jan. 2016.
- [19] A. Rittiplang, W. Pijitrojana, and K. Daroj, “Low-frequency wireless power transfers using modified parallel resonance matching at a complex load,” *KKU Engineering Journal*, vol. 43, no. 4, pp. 184-188, Oct.-Dec. 2016.
- [20] W. Amasiri and W. Pijitrojana “Development of in-motion wireless power transfer test bed platform for wireless electric vehicle charger,” *Thammasat International Journal of Science and Technology*, vol. 22, no. 2, Apr.-Jun. 2017.
- [21] G. Duan, X. Zhao, S. W. Anderson, and X. Zhang, “Boosting magnetic resonance imaging signal-to-noise ratio using magnetic metamaterials,” *Communications Physics*, vol. 2, no. 1, pp. 1-8, 2019.
- [22] J. P. C. Smeets, T. T. Overboom, J. W. Jansen, and E. A. Lomonova, “Comparison of position-independent contactless energy transfer systems,” *IEEE Trans. Power Electron.*, vol. 28, no. 4, pp. 2059–2067, Apr. 2013.
- [23] S. Assaworarith and S. Fan, “Robust and efficient wireless power transfer using a switch-mode implementation of a nonlinear parity–time-symmetric circuit,” *Nature Electronics*, vol. 546, pp. 387-390, 2017.

Jiropast Suakaew, received the master of engineering degree in Data Storage Technology from King Mongkut's Institute of Technology Ladkrabang, Thailand, the master of engineering degree in Nuclear Engineering from Chulalongkorn University, Thailand, the Ph.D. degree in Electrical Engineering, Thammasat School of Engineering, Thammasat University, Pathumthani, Thailand. His current interests are Metamaterials, Wireless Power Transfer systems. He is currently working at Seagate Technology, Thailand.

Wanchai Pijitrojana, received the Ph.D. degree in Optoelectronics from King's College, University of London, UK. He is currently a lecturer in the Electrical and Computer Department, Thammasat School of Engineering, Thammasat University, Pathumthani, Thailand. He is the head of Quantum Technology and Electromagnetics Research Group. His current research interests are Quantum Technology, Optical System Design, Wireless Power Transfer System and design, Photonic Band Gap Materials and Metamaterials, Optics both on Applications and Theory, and Nonlinear and Quantum Optics.